

Supporting Information

**Machine Learning on Deconstructing Contributions of Atomic Characterizations to
Hybridization Determined Electron Transfer in Perovskite Catalyst**

Jun Zhu,¹ Mengdan Song,¹ Qiling Qian,¹ Yang Yue,² Guangren Qian,² Jia Zhang,^{1,*}

¹ SHU Center of Green Urban Mining & Industry Ecology, School of Environmental and Chemical Engineering, Shanghai University, No. 381 Nanchen Road, Shanghai 200444, P. R. China;

² MGI of Shanghai University, Xiapu Town, Xiangdong District, Pingxiang City, Jiangxi, 337022, P. R. China;

Corresponding authors

* E-mail: irujam@t.shu.edu.cn.

eXtreme Gradient Boosting Regression (XGBR)

XGB is a decision tree ensemble algorithm developed by Tianqi Chen et al.

$$L^{(t)} = \sum_{i=1}^n l(y_i, \hat{y}_i^{t-1} + f_t(X_i)) + \Omega(f_t) \quad (13)$$

$l(y_i, \hat{y}_i^{t-1})$ represents the loss function between y_i and \hat{y}_i^{t-1} , which can be defined

by oneself. Regression problems generally use square error. y_i represents the true value of sample i . \hat{y}_i^{t-1} represents the predicted value of the top $t-1$ decision trees for sample i . $f_t(X_i)$ represents the predicted value of the t -th decision tree for sample i . $\Omega(f_t)$ represents the complexity of the t -th tree model. X_i represents the feature vector representing sample i .

In other words, when there are k trees, the predicted value for sample i is equal to the predicted value of the top $k-1$ decision trees plus the predicted value of the k -th tree. Then the objective function is

$$\text{obj} = \sum_{i=1}^n (l(y_i, \hat{y}_i^{k-1}) + f_k(X_i)) + \sum_{j=1}^{k-1} \Omega(f_j) + \Omega(f_k) \quad (14)$$

$$\sum_{j=1}^{k-1} \Omega(f_j)$$

The complexity of the previous tree is known, so $\sum_{j=1}^{k-1} \Omega(f_j)$ is the constant term.

The next step is to minimize the objective function and simplify formula (14) using Taylor expansion:

$$\text{Obj} = \sum_{i=1}^n (l(y_i, \hat{y}_i^{k-1}) + g_i f_k(X_i) + \frac{1}{2} h_i f_k^2(X_i)) + \Omega(f_k) \quad (15)$$

$$g_i = \frac{\partial l(y_i, \hat{y}_i^{k-1})}{\partial \hat{y}_i^{k-1}}, \quad h_i = \frac{\partial^2 l(y_i, \hat{y}_i^{k-1})}{\partial (\hat{y}_i^{k-1})^2}$$

are first and second derivatives of $l(y_i, \hat{y}_i^{k-1})$,

respectively.

$$\sum_{i=1}^n l(y_i, \hat{y}_i^{k-1})$$

The first term in formula (15) is the sum of the errors of the top k-1 trees. When we train the k-th tree, the error of the top k-1 trees is known and can be regarded as a constant, so we will temporarily round it off in the objective function.

Therefore, the objective function becomes a function of $f_k(X_i)$, $f_k(X_i)$ is a function of the output parameter w of the leaf node, converting the objective function into a function of w .

$$\begin{aligned} \text{Obj} &= \sum_{i=1}^n \left(g_i W_k(X_i) + \frac{1}{2} h_i W_k^2(X_i) \right) + \gamma T + \frac{1}{2} \lambda \sum_{j=1}^T w_j^2 \\ &= \sum_{j=1}^T \left(w_j \sum_{i \in I_j} g_i + \frac{1}{2} w_j^2 \sum_{i \in I_j} (h_i + \lambda) \right) + \gamma T \# (16) \end{aligned}$$

T represents the number of leaf nodes, I_j represents the sample in the j-th leaf node, λ and γ are hyperparameter. λ is the penalty coefficient for the weight w , and γ is the complexity parameter.

$$G_i = \sum_{i \in I_j} g_i, H_i = \sum_{i \in I_j} h_i$$

When

$$\text{obj} = \sum_{j=1}^T \left(w_j G_j + \frac{1}{2} w_j^2 (H_j + \lambda) \right) + \gamma T \# (17)$$

j is the j-th leaf node, and i is still the i-th sample. Obviously, formula (17) is about the quadratic function of w_j . In order to find the optimal objective function value, the

derivative of w_j is taken. When $w_j = -\frac{G_j}{H_j + \lambda}$, the objective function achieves the optimal value.

$$\mathsf{obj}_{\min} = - \frac{1}{2} \sum_{j=1}^T \frac{G_j^2}{H_j + \lambda} + \gamma T~\#(18)$$

Bayesian Global Optimization Functions

1. Probability of improvement (PI), quantifying the observation value of x may increase the probability of the current optimal objective function value, the acquisition function is as follows:

$$a_t(x, D_{1:t}) = p(f(x) \leq v^* - \xi) = \varphi\left(\frac{v^* - \xi - u_t(x)}{\sigma_t(x)}\right) \#(19)$$

v^* represents the current optimal functional value, $\varphi(\cdot)$ is the standard normal distribution cumulative density function, ξ is the equilibrium parameter (used to balance the relationship between local and global searches, usually set manually).

When near the current optimal solution, the value is large, and when far from the current optimal solution, the value is small. Although the PI strategy can select the evaluation point with the highest probability of improvement, it considers all improvements to be equal and only reflects the probability of improvement without reflecting the magnitude of the improvement.

2. Expected Improvement (EI), the acquisition function of EI includes PI, which integrates the probability of improvement and reflects different amounts of improvement:

$$a_t(x, D_{1:t}) = \begin{cases} (v^* - u_t(x))\varphi\left(\frac{v^* - u_t(x)}{\sigma_t(x)}\right) + \sigma_t(x)\varphi\left(\frac{v^* - u_t(x)}{\sigma_t(x)}\right), & \sigma_t(x) > 0 \\ 0, & \sigma_t(x) = 0 \end{cases} \#(20)$$

The EI strategy can also include the balance parameter ξ to further handle the relationship between local and global variables:

$$a_t(x, D_{1:t}) = \begin{cases} (v^* - \xi - u_t(x))\varphi\left(\frac{v^* - \xi - u_t(x)}{\sigma_t(x)}\right) + \sigma_t(x)\varphi\left(\frac{v^* - \xi - u_t(x)}{\sigma_t(x)}\right), & \sigma_t(x) > 0 \\ 0, & \sigma_t(x) = 0 \end{cases} \quad (21)$$

3. Upper confidence bound (UCB), maximizing the upper confidence level of the estimated value of the objective function:

$$a_t(x, D_{1:t}) = u_t(x) + \sqrt{\beta_i \sigma_t(x)} \quad (22)$$

β_i balances expectation and variance.

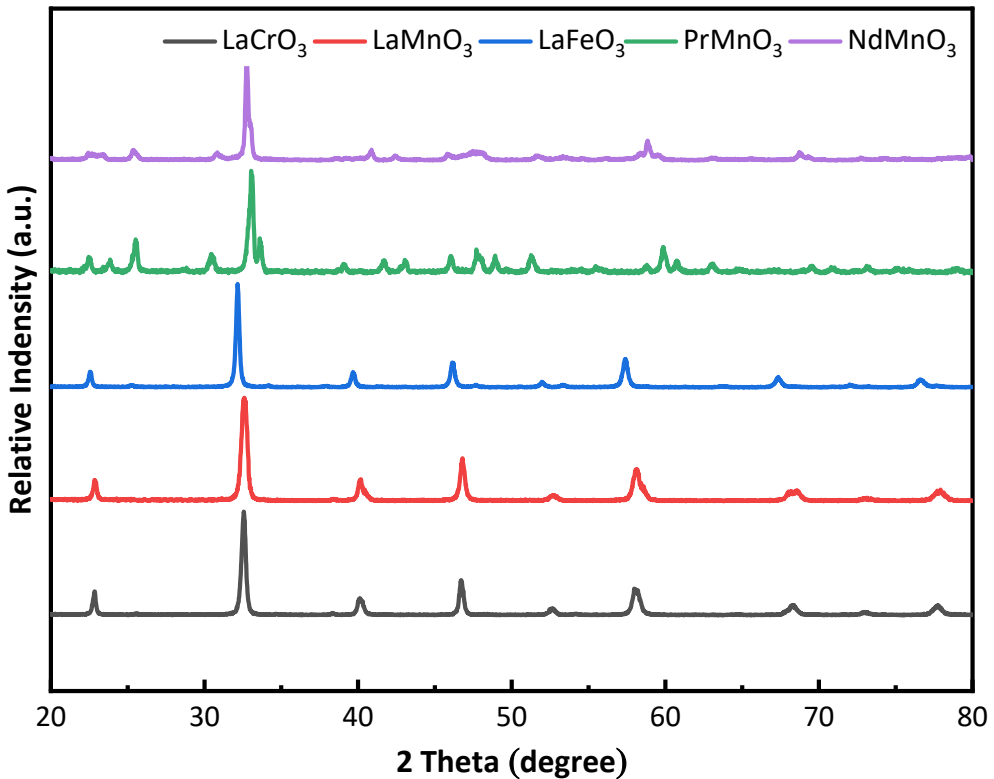


Fig. S1. XRD of synthesized perovskites.

Crystal phases of the synthesized materials were LaCrO₃¹, LaMnO₃², LaFeO₃³, PrMnO₃⁴, and NdMnO₃⁵, respectively.

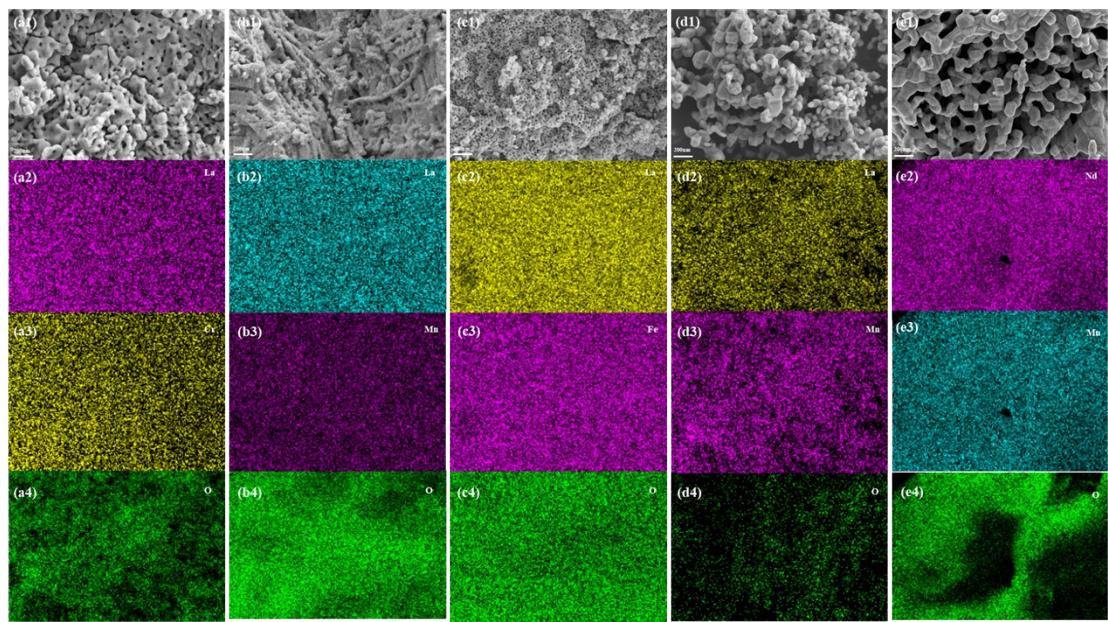


Fig. S2. (a1) SEM image, (a2) La, (a3) Cr, and (a4) O mappings of LaCrO₃. (b1) SEM image, (b2) La, (b3) Mn, and (b4) O mappings of LaMnO₃. (c1) SEM image, (c2) La, (c3) Fe, and (c4) O mappings of LaFeO₃. (d1) SEM image, (d2) Pr, (d3) Mn, (d4) O mappings of PrMnO₃. (e1) SEM image, (e2) Nd, (e3) Mn, (e4) O mappings of NdMnO₃.

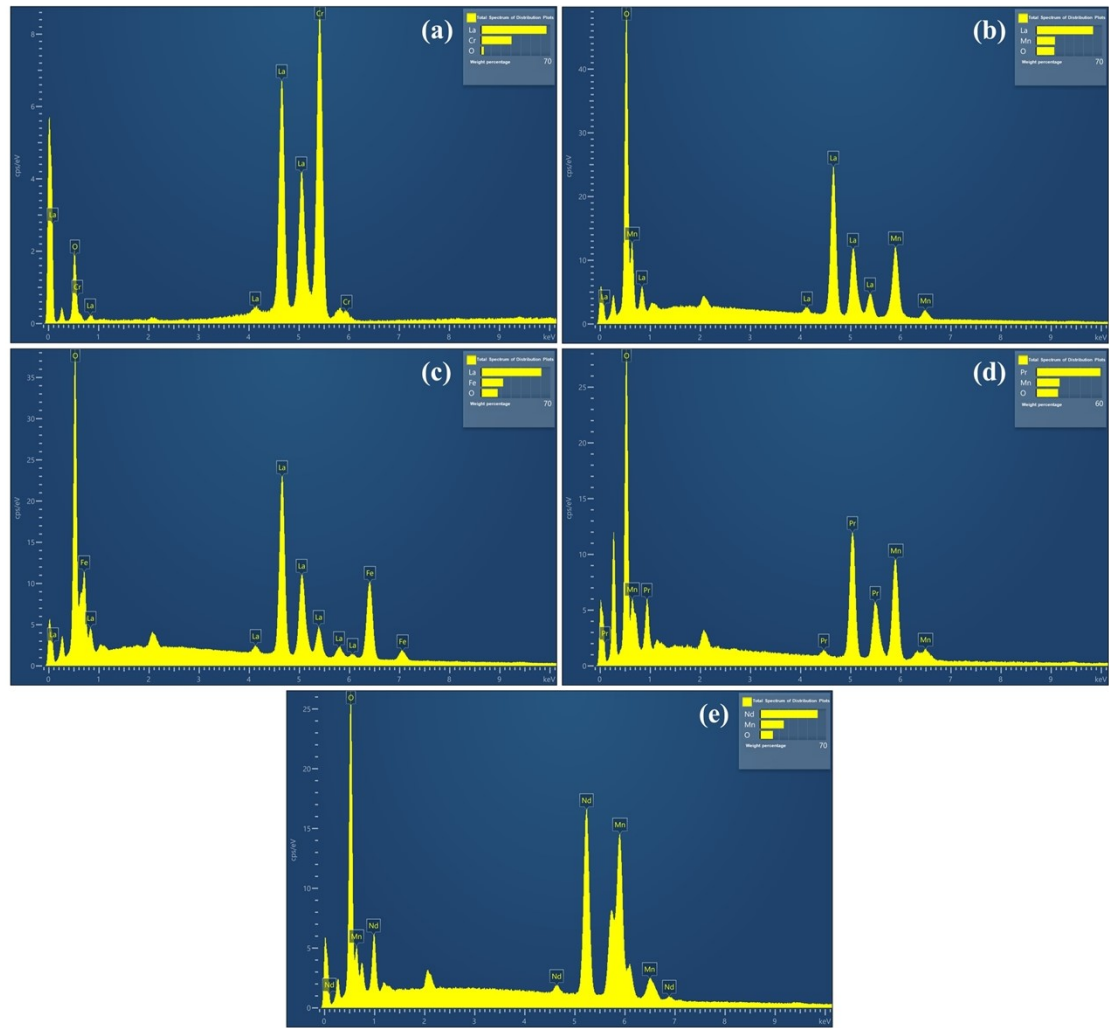


Fig. S3. SEM-EDS of (a) LaCrO_3 , (b) LaMnO_3 , (c) LaFeO_3 , (d) PrMnO_3 , and (e) NdMnO_3

Table S1. The average molar composition of each element in the perovskites

	TV of A	IV of A	EV of A	TV of B	IV of B	EV of B	TV of O	EV of O
LaCrO_3	20	47.6	35.6	20	52.4	43.3	60	21.1
LaMnO_3	20	45.7	16.8	20	54.3	14.5	60	68.7
LaFeO_3	20	48.6	18.0	20	51.4	16.6	60	65.4
PrMnO_3	20	40.4	15.7	20	59.6	14.4	60	69.9
NdMnO_3	20	45.6	19.8	20	54.4	21.5	60	58.7

TV, Theoretical value (%)

IV, ICP value (%)

EV, SEM-EDS value (%)

Table S2. Feature values and labels (toluene conversion at 330°C) of typical perovskites.

	EVDW _B	AN _A	PCR _A	D _d	Label (%)
LaCrO ₃	2.23	57	1.8	27.87	68.25
LaMnO ₃	2.25	57	1.8	26.72	99.13
LaFeO ₃	2.27	57	1.8	31.07	26.91
PrMnO ₃	2.25	59	1.76	14.98	79.07
NdMnO ₃	2.25	60	1.74	14.69	71.09

Table S3. Textural properties of the perovskites

	BET surface area (m ² ·g ⁻¹)	Total pore volume (cm ³ ·g ⁻¹)
LaCrO ₃	7.0	0.064
LaMnO ₃	14.7	0.098
LaFeO ₃	16.3	0.121
PrMnO ₃	7.6	0.022
NdMnO ₃	6.4	0.019

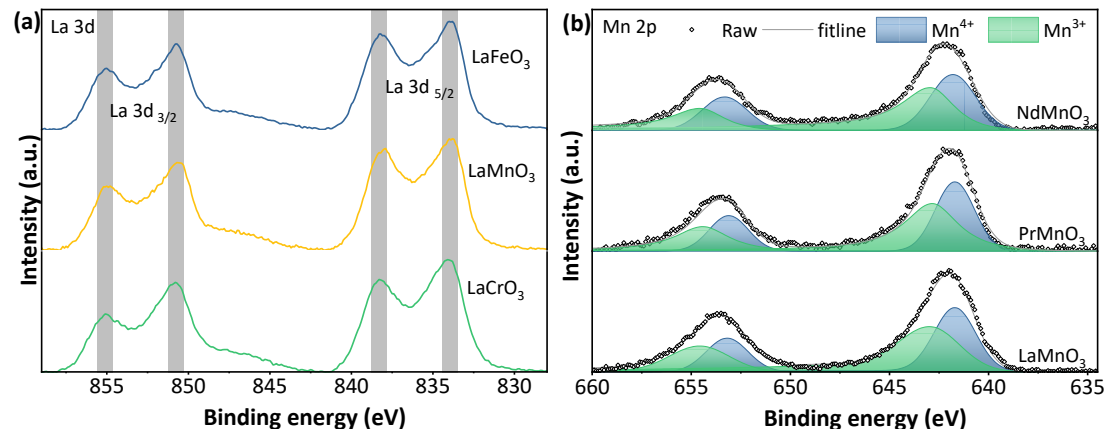


Fig. S4. XPS spectra for (a) La 3d of LaCrO₃, LaMnO₃, and LaFeO₃; (b) Mn 2p of LaMnO₃, PrMnO₃, and NdMnO₃.

Table S4. Fitting results of O1s XPS and H₂-TPR

	BE of O _{latt} (eV)	BE of O _{act} (eV)	Ratio of O _{act} /O _{latt}	T _{act} (°C)	S _{act} (mmol·g ⁻¹)	T _{latt} (°C)	S _{latt} (mmol·g ⁻¹)
LaCrO ₃	529.47	531.56	1.33	350	0.14	-	-
LaMnO ₃	529.40	531.60	1.49	359	1.09	834	1.08
LaFeO ₃	529.32	531.82	1.28	417	0.07	≥1000	≥0.37
PrMnO ₃	529.69	531.84	1.43	517	0.28	739	1.30

NdMnO₃ 529.80 531.88 1.35 472 0.34 789 1.37

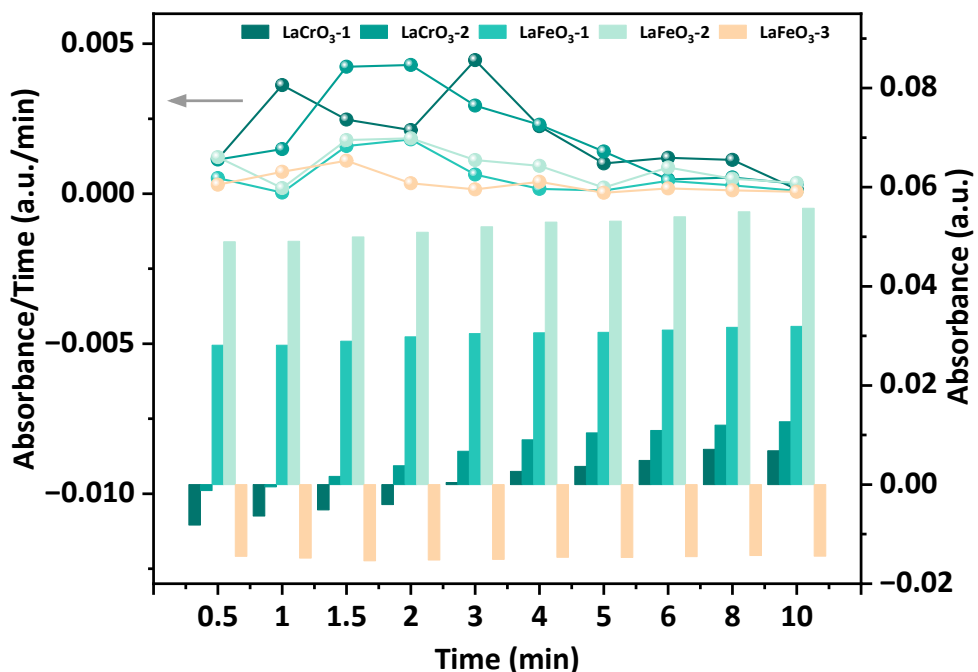
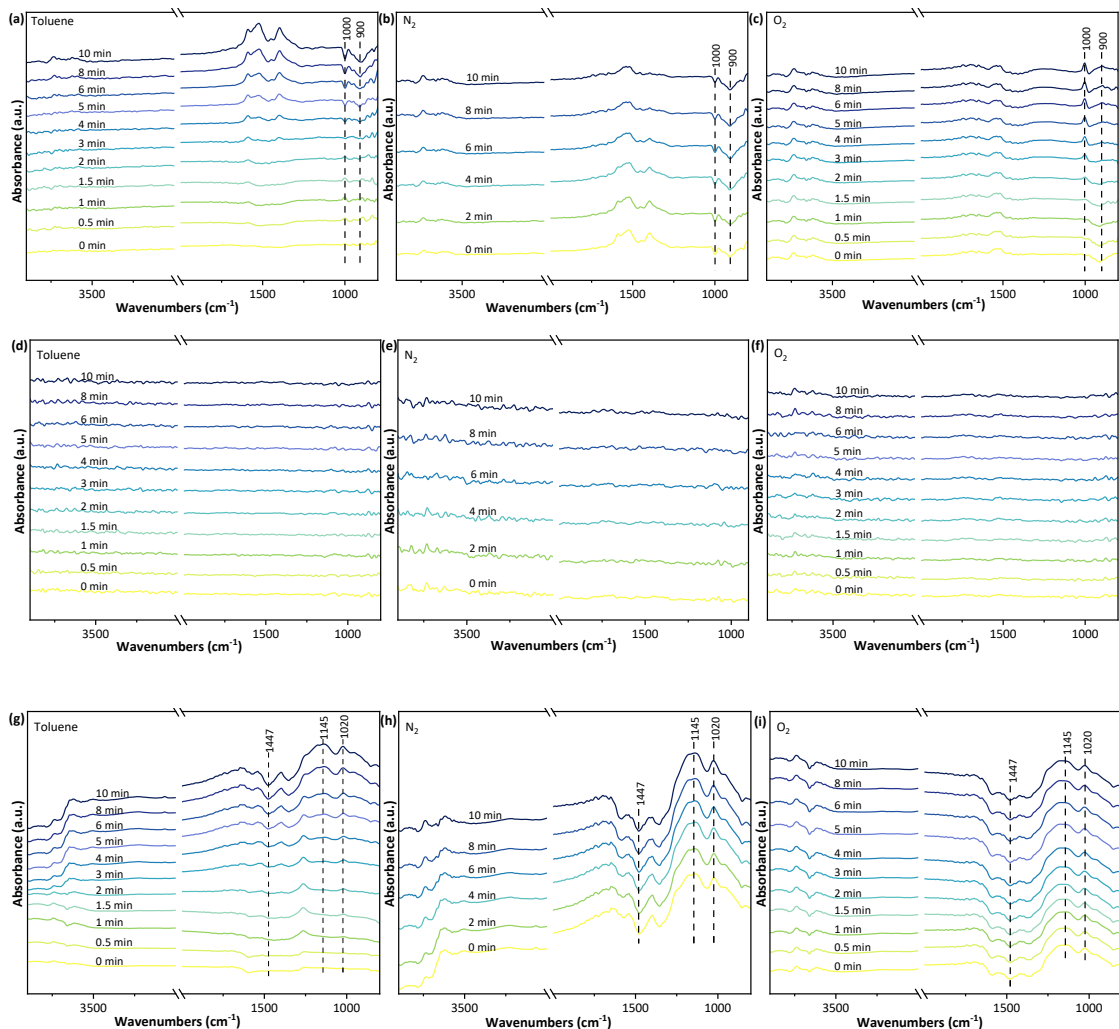


Fig. S5. DRIFTS of LaCrO₃ (**a-c**), LaMnO₃ (**d-f**), and LaFeO₃ (**g-i**). Changing rates of intermediate peaks (**j**).

Fig. S5a-S5i shows the DRIFTS of toluene-adsorbed catalysts reacted with inflowing O₂. Two peaks of LaCrO₃ (900 cm⁻¹ and 1000 cm⁻¹) were denoted as LaCrO₃-1 and LaCrO₃-2, respectively. Three peaks of LaFeO₃ (1020 cm⁻¹, 1145 cm⁻¹, and 1447 cm⁻¹) were denoted as LaFeO₃-1, LaFeO₃-2, and LaFeO₃-3, respectively. No obvious peak was recognized in LaMnO₃ since 10 min was insufficient for toluene to consume reactive oxygen species in LaMnO₃. As for the other two catalysts, the instantaneous rate of the peak change was calculated (**Fig. S5j**). The instantaneous rate of the peak in LaMnO₃ was regarded as the largest, followed by LaCrO₃ and LaFeO₃. Therefore, the difference in electron-transfer ability significantly affected the formation or disappearance of intermediates in the catalysis.

Synthesis Details

Table S5. Details of perovskite synthesis.

	Drying (°C)	Drying time (h)	Calcination (°C)	Calcination time (h)
FeMnO ₃	105	12	300/900	1/12
GdCoO ₃	105	12	350/900	2/5
GdFeO ₃	105	12	350/900	2/5
GdMnO ₃	105	12	350/900	2/5
LaAlO ₃	105	12	300/800	1/5
LaCoO ₃	105	12	650	5
LaCrO ₃	105	12	650	5
LaFeO ₃	105	12	600	8
LaMnO ₃	105	12	700	8
LaNiO ₃	105	12	650	5
NdFeO ₃	105	12	800	3
PrCoO ₃	105	12	350/900	2/5
PrFeO ₃	105	12	350/900	2/5
PrMnO ₃	105	12	350/900	2/5
PrNiO ₃	105	12	350/900	2/5
SmCoO ₃	105	12	350/900	2/5
SmFeO ₃	105	12	800	3
YFeO ₃	105	12	800	3
NdCrO ₃	105	12	350/900	2/5
NdMnO ₃	105	12	350/900	2/5
CeNiO ₃	105	12	300 (spontaneous combustion)	2
CeMnO ₃	105	12	350/900	2/5

Table S6. Descriptors of Model

Descriptor	Descriptions
AN_A	Atomic number of A-site element
AN_B	Atomic number of B-site element
R_A	Shannon effective ionic radius of A-site element
R_B	Shannon effective ionic radius of B-site element
PCR_A	Pyykkö covalent radius of A-site element
PCR_B	Pyykkö covalent radius of B-site element
CCR_A	Cordero covalent radius of A-site element
CCR_B	Cordero covalent radius of B-site element
CVDW_B	Batsanov crystallographic van der waals radius of B-site element
EVDW_B	Batsanov equilibrium van der waals radius of B-site element
AEN_B	Pearson absolute electronegativity of B-site atom
EN_B	Pearson absolute electronegativity of B-site ion
$\text{EN}_A\text{-P}$	Pauling electronegativity of A-site element
$\text{EN}_B\text{-P}$	Pauling electronegativity of B-site element
$\text{EN}_B\text{-S}$	Sanderson electronegativity of B-site element
$\text{EN}_A\text{-AR}$	Allred-Rochow electronegativity of A-site element
$\text{EN}_B\text{-AR}$	Allred-Rochow electronegativity of B-site element
$\text{EN}_B\text{-C}$	Configuration energy of B-site element
$\text{EN}_B\text{-A}$	Allred electronegativity of B-site element
$\text{EN}_A\text{-NE}$	Nagle electronegativity of A-site element
$\text{EN}_B\text{-NE}$	Nagle electronegativity of B-site element
$\text{EN}_B\text{-Sm}$	Smith electronegativity of B-site element
$\text{EN}_A\text{-MB}$	Matyevon-Batsanov of A-site element
$\text{EN}_B\text{-MB}$	Matyevon-Batsanov of B-site element
FIE_B	First ionization energy of B-site element
SIE_B	Second ionization energy of B-site element
TIE_B	Third ionization energy of B-site element
EA_B	Electron affinity of B-site element
GR_A	Group number of A-site element
GR_B	Group number of B-site element
PE_A	Period number of A-site element
PE_B	Period number of B-site element
d_B	The number of d electrons of B-site element
D_d	d electron density of B-site element
CN_O	The coordination number of O
SG	Space Group
τ	The tolerance factor
μ	Octahedral factor
FE	Formation Energy

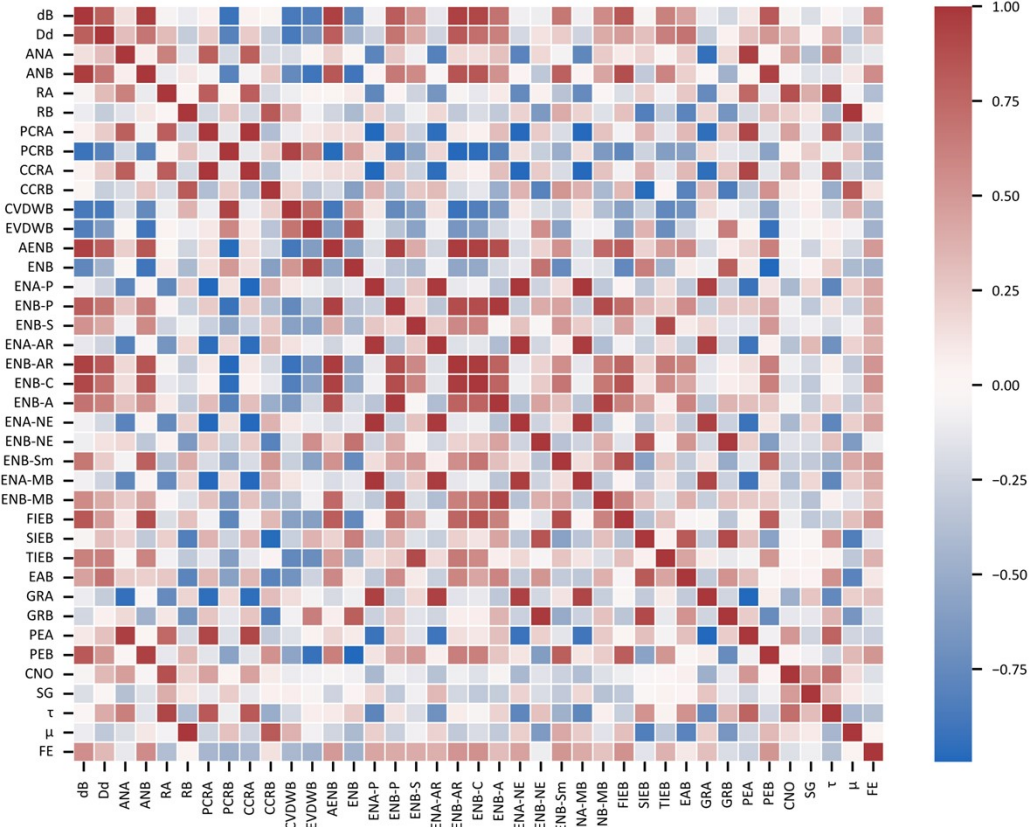


Fig. S6. Heatmap of the Pearson correlation coefficient matrix between descriptors

Electrochemical Impedance Spectroscopy

The battery had Ag/AgCl (4M KCl) reference electrode, platinum wire pair electrode, and catalyst modified glass carbon working electrode, the electrolyte was 0.1 M Na₂SO₄. Homogeneous catalyst ink was prepared by 10 mg catalyst powder, 10 mg conductive carbon, 0.1 mL Nafion solution and 1 mL of anhydrous ethanol. Then transfer it to the surface of the glassy carbon electrode and dry it in ambient air. EIS were recorded at -0.3 V vs. Ag/AgCl within a frequency range from 10⁵ to 10⁻¹ Hz using an AC voltage at a 5mV amplitude.

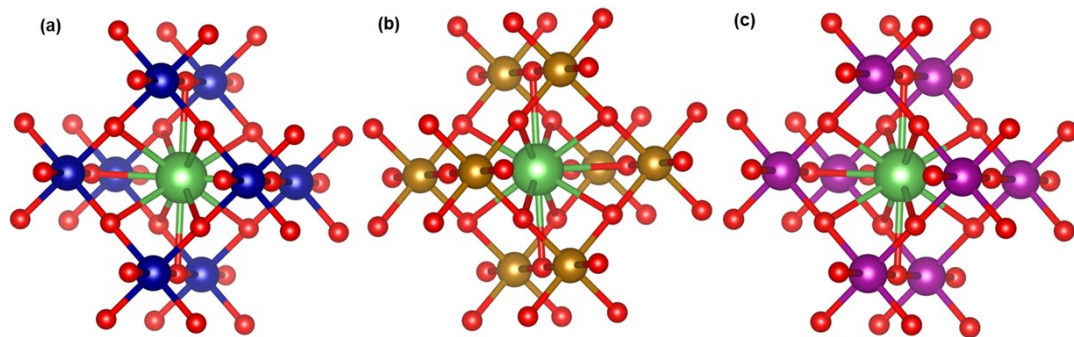


Fig. S7. LaCrO₃ (a), LaMnO₃ (b), LaFeO₃ (c) perovskite structure model.

References

1. H. Zhao, Q. Zhu, X. Ye, L. Wang and S. Dong, *Coatings*, 2024, **14**.
2. Z.-X. Wei, L. Wei, L. Gong, Y. Wang and C.-W. Hu, *Journal of Hazardous Materials*, 2010, **177**, 554-559.
3. S. Afzal, X. Quan and J. Zhang, *Applied Catalysis B: Environmental*, 2017, **206**, 692-703.
4. S. Chen, Y. Hao, R. Chen, Z. Su and T. Chen, *Journal of Alloys and Compounds*, 2021, **861**.
5. Y. Wang, H. Wang, W. Tan and D. Huo, *Journal of Applied Physics*, 2022, **132**.